PCCP

PAPER

View Article Online
View Journal | View Issue

Cite this: *Phys. Chem. Chem. Phys.*, 2024, **26**, 8089

Breaking the plane: B_5H_5 is a three-dimensional structure†

Gerardo Hernández-Juárez,[a] Jorge Barroso,[b] Alejandro Vásquez-Espinal,[c] Filiberto Ortíz-Chi,[d] William Tiznado,[e] Fernando Murillo*[a] and Gabriel Merino*[a]

Received 3rd January 2024,
Accepted 16th February 2024

DOI: 10.1039/d4cp00029c

rsc.li/pccp

In this study, we delved into the structure of B_5H_5 and questioned some of its accepted assumptions. By exploring the potential energy surface, we found a new three-dimensional structure as the global minimum. This finding is in contrast with the previously hypothesized planar and cage-like models. Our exploration extends to the kinetic stability of various B_5H_5 isomers, offering insights into the dynamic behavior of these molecules.

Introduction

Even though $B_5H_5^{2-}$ has not yet been synthetized, it is expected to assume a D_{3h} form, a conjecture first formulated by Lipscomb and coworkers in 1961,[1–3] and later rationalized through the Wade-Mingos rules.[4,5] In 2000, Schleyer and coworkers explored the geometric and electronic implications of electron removal from $B_5H_5^{2-}$ to elucidate the structure of the neutral B_5H_5.[6] Upon optimization, the initial trigonal bipyramidal form with D_{3h} symmetry transitioned to a C_{4v} square pyramid, keeping the five B–H units intact in B_5H_5 (Fig. 1). This transformation from trigonal bipyramid to square pyramid was rationalized *via* the pairing principle of incompletely filled degenerate orbitals.[6] However, McKee[7] identified a C_s structure, characterized as a BH_2^+ and $B_4H_3^-$ complex, which is energetically more favorable than the C_{4v} square pyramidal isomer by 9.8 kcal mol^{-1} at the B3LYP/6-31G(d) level. This preferred structure is a trapezoid with three B atoms at the base and two above, incorporating two terminal B–H bonds, a B–H–B bridge, a BH_2 group, and a bare boron (see Fig. 1),[7] mirroring the planar form of B_5^- and neutral B_5.[8,9]

In our quest to understand the structural transformations induced by the removal of two electrons from the dianions of borohydrides, denoted by the formula $B_nH_n^{2-}$, we explored the potential energy surfaces (PESs) of all borohydrides in the series from n = 5 to 12. Our preliminary screening revealed that for nearly all these dianions, the removal of two electrons result in insignificant structural changes. Nonetheless, two exceptions were identified: $B_{12}H_{12}$ and B_5H_5. While the former case has been previously reported by us,[10] our focus now shifts to B_5H_5. Contrary to prior assumptions, our results show that the global minimum structure of B_5H_5 is not quasi-planar but rather an asymmetrical three-dimensional form.

Computational details

The systematic exploration of the PES of B_5H_5 in both its singlet and triplet states was carried out through a modified genetic algorithm as implemented in GLOMOS.[11] Details on GLOMOS are documented elsewhere.[12] An initial screening was performed at the PBE0/def2-SVP level.[13,14] Isomers within a 50 kcal mol^{-1} range were re-minimized and characterized at the TPSS-D3/def2-TZVP level.[14,15] The stationary points were further characterized

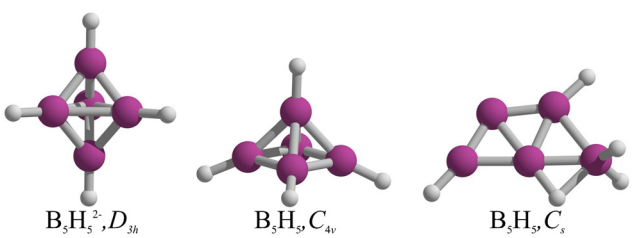

Fig. 1 The structures proposed for $B_5H_5^{2-}$ (D_{3h}) and B_5H_5 (C_{4v} and C_s).

[a] *Departamento de Física Aplicada, Centro de Investigación y de Estudios Avanzados, Unidad Mérida. Km 6 Antigua Carretera a Progreso. Apdo. Postal 73, Cordemex, 97310, Mérida, Yuc., Mexico. E-mail: gmerino@cinvestav.mx, fernando.murillo@cinvestav.mx*
[b] *Department of Chemistry, Clemson University, Clemson, South Carolina 29625, USA*
[c] *Química y Farmacia, Facultad de Ciencias de la Salud, Universidad Arturo Prat, Casilla 121, Iquique 1100000, Chile*
[d] *CONAHCYT-División Académica de Ciencias Básicas, Universidad Juárez Autónoma de Tabasco, Cunduacán 86690, Tabasco, Mexico*
[e] *Departamento de Ciencias Químicas, Facultad de Ciencias Exactas, Universidad Andres Bello, República 498, Santiago, Chile*

† Electronic supplementary information (ESI) available. See DOI: https://doi.org/10.1039/d4cp00029c

by harmonic vibrational frequency analysis at the same level. The interconversion pathways for lower-energy minima were elucidated and the corresponding transition states (TS) connecting the local minima were confirmed by intrinsic reaction coordinate (IRC) computations. Relative Gibbs free energies, including entropic and thermal corrections at 298.15 K, were computed at the CCSD(T)[16]/aug-cc-pVTZ//TPSS-D3/def2-TZVP level. Additionally, the stability of the wave function and the T_1 diagnostic for each isomer were evaluated, indicating stable wave functions across all localized minima with T_1 values below 0.02 for the singlet systems and less than 0.023 for the triplets (see Table S1, ESI†). This suggests that monodeterminantal approaches, such as DFT and CCSD(T), reliably represent the structure and energetics of these isomers. All these computations were performed using Gaussian 16.[17]

Chemical bonding was examined using Wiberg bond indices (WBIs) and natural population analysis (NPA) *via* the NBO 6.0[18] partitioning scheme. Furthermore, the adaptive natural density partitioning (AdNDP) approach,[19] as implemented in Multiwfn,[20] provided further insights into the chemical bonding, describing electronic structures in terms of *n*-center, two-electron (*nc*-2e) bonds, recovering Lewis concepts such as lone pairs, **2c-2e** bonds, and delocalized bonds.

The dynamic behavior was studied using Born–Oppenheimer molecular dynamics (BO–MD)[21] at 900 K for 30 ps, employing a 1 fs time step and a Nosé–Hoover chain thermostat for temperature control,[22–24] using deMon-2k[25] at the PBE0/DZVP[26] level. The chosen temperature, while is not real in the macroscopic sense, was selected to regulate the total kinetic energy of the atoms, ensuring they possess enough energy to overcome energy barriers and allow for isomer interconversions at realistic simulation times.

Results

The lowest energy structures of B_5H_5 in both singlet and triplet states are shown in Fig. 2. We identified two structures, **1** and **2**, that are energetically more favorable than McKee's proposed structure, **3**.[7] The global minimum, **1**, is a three-dimensional entity with C_1 symmetry, characterized by four terminal B–H bonds, a B–H–B bridge, and a bare boron atom. Structure **2**, which is only 0.7 kcal mol^{-1} higher than **1** in Gibbs free energy (computed at CCSD(T)/aug-cc-pVTZ//TPSS-D3/def2-TZVP), adopts a trapezoidal boron skeleton with three B–H units and a $-BH_2$ group located at one vertex of the larger base, adopting a C_s symmetry. McKee's structure (**3**), less favorable by 1.7 kcal mol^{-1} compared to **1**, shares a trapezoidal shape with **2** but includes a hydrogen atom bridging the central boron and the $-BH_2$ group. Structure **4**, which is 3.0 kcal mol^{-1} higher in energy than **3**, possesses a distinctive trapezoidal shape with an out-of-plane BH unit. Structures **5**, **7**, **8**, **13**, and **14**, characterized by pyramidal boron skeletons, are between 6.7 to 38.9 kcal mol^{-1} higher in Gibbs free energy than **1**, with **7** corresponding to Schleyer's C_{4v} structure. Three C_s-symmetry structures, **6**, **9**, and **10**, consist of a B_4 skeleton with a $-BH_2$ unit and a bridging hydrogen on a B–B bond, ranging from 6.8 to 17.0 kcal mol^{-1} above **1** in Gibbs free energy. Isomers **11** and **12** adopt a cage-like structure ($\Delta G > 17.0$ kcal mol^{-1}), albeit with one incomplete face. Specifically, structure **12** is a trapezoid with two B–H–B bridges with an out-of-plane hydrogen atom in one bridge. The lowest-energy triplets, **13** and **14**, have ΔG values more than 20 kcal mol^{-1} above **1**. So, the putative global minimum for B_5H_5 is not planar but a three-dimensional structure.

WBI analysis identifies two distinct ranges for B–H bond distances, as summarized in Table 1. Isomers **2**, **5**, and **7**, each containing five B–H units, display high average WBI_{B-H} of

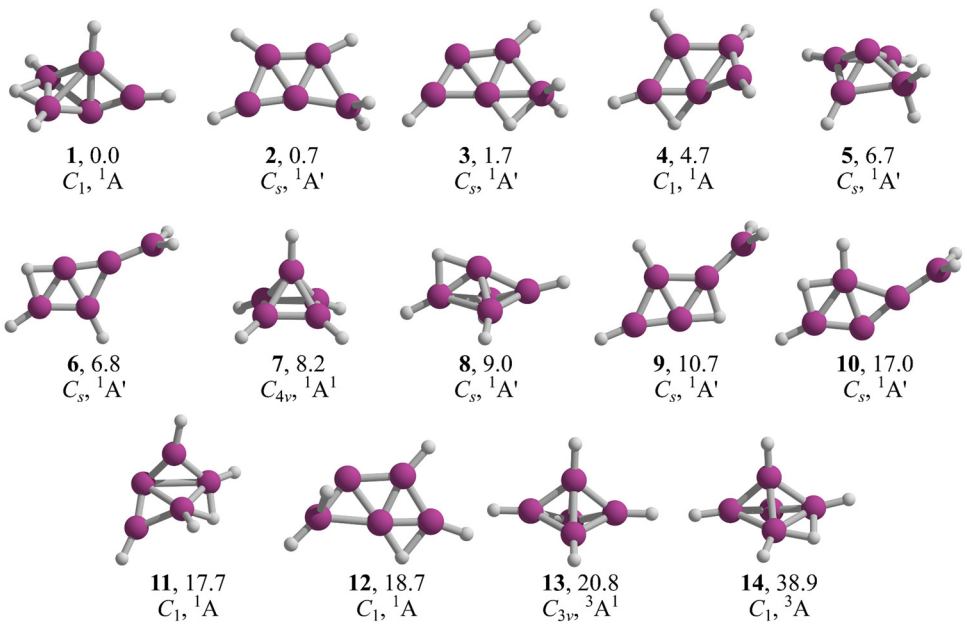

Fig. 2 TPSS-D3/def2-TZVP low-lying energy structures of B_5H_5. Relative Gibbs free energies at the CCSD(T)/aug-cc-pVTZ//TPSS-D3/def2-TZVP level are in kcal mol^{-1}.

Table 1 Average Wiberg bond indices and average bond lengths r_{B-B} and r_{B-H} in Å computed at the TPSS-D3/def2-TZVP level

Isomer	r_{B-H}	r_{B-B}	WBI_{BH}	WBI_{BB}
1	1.22	1.67	0.79	0.85
2	1.19	1.69	0.94	0.80
3	1.24	1.67	0.78	0.89
4	1.23	1.66	0.78	0.87
5	1.19	1.72	0.95	0.77
6	1.24	1.62	0.79	1.00
7	1.19	1.71	0.95	0.74
8	1.23	1.71	0.79	0.78
9	1.24	1.63	0.79	0.99
10	1.24	1.65	0.78	1.01
11	1.23	1.71	0.78	0.84
12	1.28	1.65	0.66	0.93

around 0.95 and show the shortest average B–H bond lengths, approximately 1.19 Å. In contrast, the presence of **3c-2e** B–H–B interactions increases average B–H bond distances and lowers the average WBI_{B-H} values. An extreme case is structure **12**, which features two B–H–B bonds, leading to a WBI of 0.66. Regarding B–B bonds, planar structures **6**, **9**, and **10** show the highest average WBI_{B-B} values (nearly 1.0), contrasting with Schleyer's isomer, which has the lowest (WBI_{B-B} = 0.74). **6**, **9**, and **10** each contain a **2c-2e** B–B bond connecting a BH_2 unit to the B_4H_3 fragment. The formation of the BH_2 unit induces electronic redistribution within the B_4 rhombus, shortening several B–B distances to almost 1.55 Å. In contrast, an increase in the number of multicenter boron bonds correlates with elongated B–B bond lengths and higher WBI_{B-B}, the C_{4v} form being the extreme case (*vide infra*).

Let us analyze the bonding properties of **1**, **3**, and **7** (the global minimum, McKee's isomer, and Schleyer's cage-pyramidal structure, respectively). As depicted in Fig. 3, each has five **2c-2e** σ-bonds. Isomers **1** and **3** are composed of four **2c-2e** B–H bonds and one B–B bond, while in **7**, all are B–H bonds. Isomer **1** features three **3c-2e** bonds (one in a B_2H ring and two in a B_3 ring), in contrast to **3** and **7**, which have four **3c-2e** bonds. Specifically, isomer **3** includes a **3c-2e** B_2H bond and another in a B_3 ring. In isomer **7**, **3c-2e** σ-bonds are found within the B_3 rings of the pyramid's four triangular faces. Each isomer also contains a delocalized **4c-2e** bond in a B_4 unit. Distinctly, the B_5 skeleton in **1** is stabilized by a **5c-2e** bond, absent in **3** and **7**, contributing to its enhanced stability.

The stabilization of **1** is further clarified when examining the chemical bonding in the dianion $B_5H_5^{2-}$, which has 22 electrons.[27] Ten of these electrons are in the five **2c-2e** B–H σ-bonds, leaving twelve for B–B bonding, including three **3c-2e** and three delocalized **4c-2e** σ-bonds.[27] In contrast, neutral B_5H_5 requires different bonding configurations. **7** has five **2c-2e** σ-bonds exclusively for B–H bonds, one more than isomers **1** and **3**. This leaves ten electrons for B–B bonds in **7**, while **1** and **3** each allocate twelve electrons to B–B bonds, similar to the dianion. Therefore, **1** and **3** are capable to maintain twelve electrons for keeping the boron skeleton in B_5H_5, resulting in higher relative stability.

The kinetic stability of isomers **3** and **7**, in their isomerization to **1**, is detailed in Fig. 4. Isomer **3** converts to **1** through a one-step pathway (Fig. 4a), with a high activation barrier ($\Delta G^{\ddagger}$ = 26.3 kcal mol^{-1}), indicating that **3** is kinetically stable. In contrast, the transformation of **7** to **1** follows a stepwise mechanism with low barriers *via* intermediates **4** and **2** (Fig. 4b). Initially, a hydrogen atom migrates from the pyramid's apex to its base, forming a B2–H–B3 bridge and leading to the cleavage of the B1–B2 bond. This results in the quasi-planar structure of **4**, crossing a small energy barrier ($\mathbf{TS_{7\text{-}4}}$, $\Delta G^{\ddagger}$ = 1.3 kcal mol^{-1}). The subsequent conversion of **4** to **2** involves a hydrogen atom shift towards B2, forming a terminal BH_2 group ($\mathbf{TS_{4\text{-}2}}$, $\Delta G^{\ddagger}$ = 4.9 kcal mol^{-1}). The final step from **2** (a quasi-planar structure) to **1** (a three-dimensional structure) implies the formation of the B2–H–B4 bridge and the B2–B5 bond, involving a barrier of 6.9 kcal mol^{-1} ($\mathbf{TS_{2\text{-}1}}$). Given that **7** isomerizes to **1** *via* a stepwise mechanism with achievable energy barriers, **7** is considered kinetically unstable.

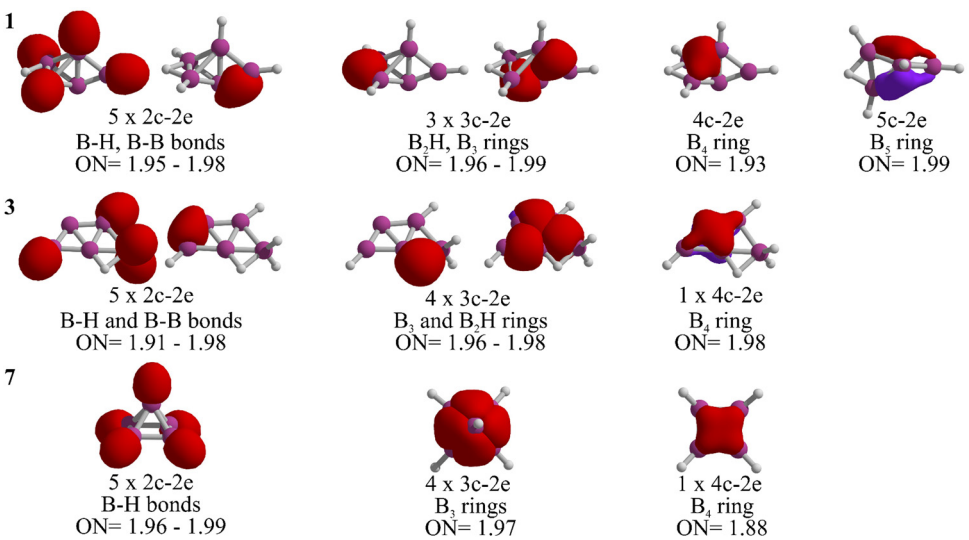

Fig. 3 AdNDP analysis for **1**, **3**, and **7** at the TPSS/def2-TZVP level. Occupation numbers (ON) in |e|.

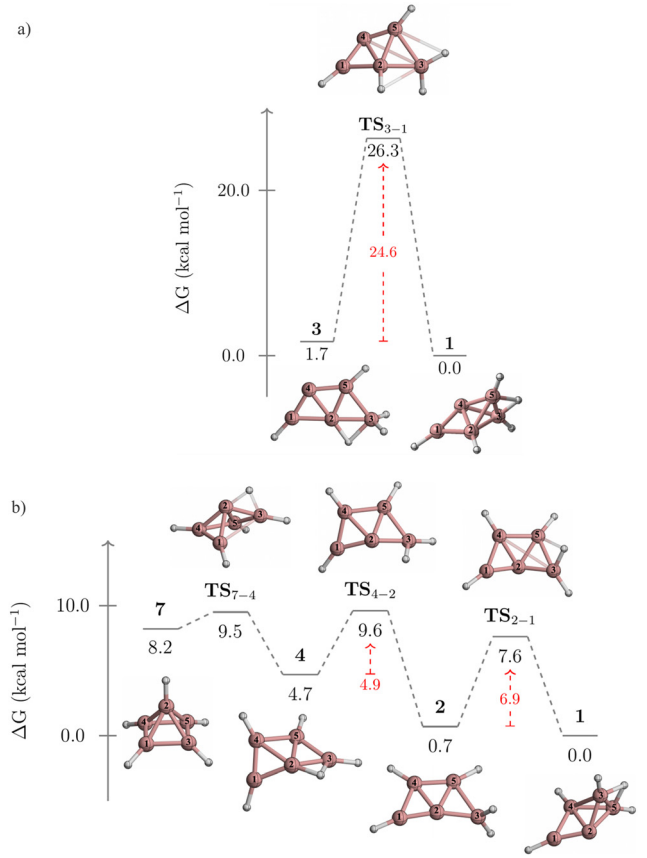

Fig. 4 Gibbs free energy profile for the conversions of (a) **3** to **1**, and (b) **7** to **1** computed at the CCSD(T)/aug-cc-pVTZ//TPSS/def2-TZVP level.

Two alternative mechanisms for the isomerization of **3** to **1** were explored. Both mechanisms involve a stepwise process, with higher activation barriers than the concerted pathway (Fig. S1 and S2, ESI†). The first pathway begins with converting **3** into **2** *via* a 1,2-H migration from B2 to B4, before transitioning to **1** (Fig. S1, ESI†). However, the initial step has a free energy barrier of 31.8 kcal mol^{-1} ($\mathbf{TS_{3\text{-}2}}$), which is 7.2 kcal mol^{-1} higher than the barrier of the concerted pathway ($\mathbf{TS_{3\text{-}1}}$, Fig. 4a).

The second pathway initiates with the cleavage of the B2–B3 bond and the formation of a B4–H–B5 bond, leading to **9** (Fig. S2, ESI†). The activation barrier for this initial step ($\mathbf{TS_{3\text{-}9}}$) is 14.9 kcal mol^{-1}. Next, **9** is converted to **6** through a double hydrogen rearrangement *via* $\mathbf{TS_{9\text{-}6}}$. This step involves breaking the B4–H–B5 bond and forming the B1–H–B2 bond with a low energy barrier ($\Delta G^{\ddagger}$ = 5.6 kcal mol^{-1}) and can be viewed as a type II-dyotropic migration.[28] The conversion from **6** to **2** ($\mathbf{TS_{6\text{-}2}}$) has an activation barrier of 27.5 kcal mol^{-1}. As in the previous stepwise pathway, this process concludes with converting **2** to **1**. Note that the barrier of $\mathbf{TS_{6\text{-}2}}$, acting as the rate-determining step, is 2.9 kcal mol^{-1} higher than that of $\mathbf{TS_{3\text{-}1}}$, indicating that these alternative routes are energetically less favorable.

To gain deeper insight into the isomerization processes from **3** to **1** and **7** to **1**, Born–Oppenheimer molecular dynamics simulations were conducted at 900 K for 30 ps, beginning with structures **3** and **7** (see the Movie S1 and S2 in the ESI†). Isomer **3** displayed minor distortions while preserving its planar structure throughout the simulation, confirming its kinetic stability in line with its high activation barrier (Fig. 4a and Movie S1, ESI†). In the case of isomer **7**, a transformation occurs at 9 ps (Movie S2, ESI†), where its pyramidal cage transitions into a trapezoidal shape reminiscent of isomer **4**. This stage is characterized by the heightened mobility of hydrogen atoms around the boron-based trapezoid, leading to several structural interconversions between isomers **4** and **2** until 20 ps. When structure **2** forms, it briefly shifts to **1** but reverts to **2**. Around 23 ps, **2** undergoes bending and transitions into the stable structure of **1** with minimal distortions for the rest of the simulation. This series of events confirms the kinetic stability of both isomers **1** and **3**, as they maintain their structural integrity throughout the simulation.

Conclusion

By exploring the B_5H_5 potential energy surface, we found a three-dimensional structure that challenges the previously accepted planar model as the global minimum for this neutral borohydride. The analysis of the kinetic stability of the B_5H_5 isomers indicates that isomer **3**, suggested by Mckee, is a kinetically stable system that could potentially be experimentally detected, but it is not the global minimum. In contrast, isomer **7** (Schleyer's proposal) is likely to transform into isomer **1**, making its experimental detection in the gas phase challenging, if not impossible. Through molecular dynamics simulations, we provided detailed insights into the dynamic behavior of these molecules, enhancing our understanding of their stability under various conditions.

These findings open new avenues for re-examining the bonding and structure of boron hydrides, extending beyond theoretical interest, and possibly influencing future experimental endeavors and applications in related chemical areas.

Conflicts of interest

There are no conflicts to declare.

Acknowledgements

G. H.-J. and F. M. thank Conacyt for their PhD and postdoc fellowships, respectively. The work in Chile was supported by the National Agency for Research and Development (ANID) *via* the Fondecyt projects N° 1211128 (W. T.) and 1221019 (A. V.-E.).

References

1 W. N. Lipscomb, Extensions of the Valence Theory of Boron Compounds, *Proc. Natl. Acad. Sci. U. S. A.*, 1961, **47**(11), 1791–1795.
2 E. B. Moore, L. L. Lohr and W. N. Lipscomb, Molecular Orbitals in Some Boron Compounds, *J. Chem. Phys.*, 1961, **35**(4), 1329–1334.

3 R. Hoffmann and W. N. Lipscomb, Theory of Polyhedral Molecules. I. Physical Factorizations of the Secular Equation, *J. Chem. Phys.*, 1962, **36**(8), 2179–2189.
4 K. Wade, Structural and Bonding Patterns in Cluster Chemistry, in *Advances in Inorganic Chemistry and Radiochemistry*, Elsevier, 1976, pp. 1–66.
5 D. M. P. Mingos, A General Theory for Cluster and Ring Compounds of the Main Group and Transition Elements, *Nat. Phys. Sci.*, 1972, **236**(68), 99–102.
6 M. L. McKee, Z.-X. Wang and P. v R. Schleyer, *Ab Initio* Study of the *Hypercloso* Boron Hydrides B_nH_n and $B_nH_n^-$. Exceptional Stability of Neutral $B_{13}H_{13}$, *J. Am. Chem. Soc.*, 2000, **122**(19), 4781–4793.
7 M. L. McKee, *Ab Initio* Study of B_nH_n and $B_n(NH_2)_n$ (n = 3–6) Species. A Comparison of Classical and Nonclassical Structures, *Inorg. Chem.*, 1999, **38**(2), 321–330.
8 H.-J. Zhai, L.-S. Wang, A. N. Alexandrova and A. I. Boldyrev, Electronic Structure and Chemical Bonding of B_5^- and B_5 by Photoelectron Spectroscopy and *Ab Initio* Calculations, *J. Chem. Phys.*, 2002, **117**(17), 7917–7924.
9 J. Barroso, S. Pan and G. Merino, Structural Transformations in Boron Clusters Induced by Metal Doping, *Chem. Soc. Rev.*, 2022, **51**(3), 1098–1123.
10 G. Hernández-Juárez, A. Vásquez-Espinal, F. Murillo, A. Quintal, F. Ortíz-Chi, X. Zarate, J. Barroso and G. Merino, Unveiling the Electronic and Structural Consequences of Removing Two Electrons from $B_{12}H_{12}^{2-}$, *Dalton Trans.*, 2023, **52**(46), 17398–17406.
11 F. Ortiz-Chi and G. Merino, *GLOMOS*, Mérida, México, 2020.
12 R. Grande-Aztatzi, P. R. Martínez-Alanis, J. L. Cabellos, E. Osorio, A. Martínez and G. Merino, Structural Evolution of Small Gold Clusters Doped by One and Two Boron Atoms, *J. Comput. Chem.*, 2014, **35**(32), 2288–2296.
13 C. Adamo and V. Barone, Toward Reliable Density Functional Methods without Adjustable Parameters: The PBE0 Model, *J. Chem. Phys.*, 1999, **110**(13), 6158–6170.
14 F. Weigend and R. Ahlrichs, Balanced Basis Sets of Split Valence, Triple Zeta Valence and Quadruple Zeta Valence Quality for H to Rn: Design and Assessment of Accuracy, *Phys. Chem. Chem. Phys.*, 2005, **7**(18), 3297–3305.
15 J. Tao, J. P. Perdew, V. N. Staroverov and G. E. Scuseria, Climbing the Density Functional Ladder: Nonempirical Meta-Generalized Gradient Approximation Designed for Molecules and Solids, *Phys. Rev. Lett.*, 2003, **91**(14), 146401.
16 J. D. Watts, J. Gauss and R. J. Bartlett, Coupled-Cluster Methods with Noniterative Triple Excitations for Restricted Open-Shell Hartree–Fock and Other General Single Determinant Reference Functions. Energies and Analytical Gradients, *J. Chem. Phys.*, 1993, **98**(11), 8718–8733.
17 M. J. Frisch, G. W. Trucks, H. B. Schlegel, G. E. Scuseria, M. A. Robb, J. R. Cheeseman, G. Scalmani, V. Barone, G. A. Petersson, H. Nakatsuji, X. Li, M. Caricato, A. V. Marenich, J. Bloino, B. G. Janesko, R. Gomperts, B. Mennucci, H. P. Hratchian, J. V. Ortiz, A. F. Izmaylov, J. L. Sonnenberg, D. Williams-Young, F. Ding, F. Lipparini, F. Egidi, J. Goings, B. Peng, A. Petrone, T. Henderson, D. Ranasinghe, V. G. Zakrzewski, J. Gao, N. Rega, G. Zheng, W. Liang, M. Hada, M. Ehara, K. Toyota, R. Fukuda, J. Hasegawa, M. Ishida, T. Nakajima, Y. Honda, O. Kitao, H. Nakai, T. Vreven, K. Throssell, J. A. Montgomery Jr., J. E. Peralta, F. Ogliaro, M. J. Bearpark, J. J. Heyd, E. N. Brothers, K. N. Kudin, V. N. Staroverov, T. A. Keith, R. Kobayashi, J. Normand, K. Raghavachari, A. P. Rendell, J. C. Burant, S. S. Iyengar, J. Tomasi, M. Cossi, J. M. Millam, M. Klene, C. Adamo, R. Cammi, J. W. Ochterski, R. L. Martin, K. Morokuma, O. Farkas, J. B. Foresman and D. J. Fox, *Gaussian 16, Revision C.01*, Gaussian, Inc., Wallingford CT, 2016.
18 E. D. Glendening, C. R. Landis and F. Weinhold, NBO 6.0: Natural Bond Orbital Analysis Program, *J. Comput. Chem.*, 2013, **34**(16), 1429–1437.
19 D. Y. Zubarev and A. I. Boldyrev, Developing Paradigms of Chemical Bonding: Adaptive Natural Density Partitioning, *Phys. Chem. Chem. Phys.*, 2008, **10**(34), 5207–5217.
20 T. Lu and F. Chen, Multiwfn: A Multifunctional Wavefunction Analyzer, *J. Comput. Chem.*, 2012, **33**(5), 580–592.
21 J. M. Millam, V. Bakken, W. Chen, W. L. Hase and H. B. Schlegel, *Ab Initio* Classical Trajectories on the Born–Oppenheimer Surface: Hessian-Based Integrators Using Fifth-Order Polynomial and Rational Function Fits, *J. Chem. Phys.*, 1999, **111**(9), 3800–3805.
22 S. Nosé, A Unified Formulation of the Constant Temperature Molecular Dynamics Methods, *J. Chem. Phys.*, 1984, **81**(1), 511–519.
23 G. J. Martyna, M. L. Klein and M. Tuckerman, Nosé–Hoover Chains: The Canonical Ensemble *via* Continuous Dynamics, *J. Chem. Phys.*, 1992, **97**(4), 2635–2643.
24 W. G. Hoover, Canonical Dynamics: Equilibrium Phase-Space Distributions, *Phys. Rev. A: At., Mol., Opt. Phys.*, 1985, **31**(3), 1695.
25 A. M. Koster, G. Geudtner, A. Alvarez-Ibarra, P. Calaminici, M. E. Casida, J. Carmona-Espindola, V. D. Dominguez, R. Flores-Moreno, G. U. Gamboa, A. Goursot, T. Heine, A. Ipatov, A. de la Lande, F. Janetzko, J. M. del Campo, D. Mejia-Rodriguez, J. U. Reveles, J. Vasquez-Perez, A. Vela, B. Zuniga-Gutierrez and D. R. Salahub, *deMon2k, Version 5*, The deMon Developers, Cinvestav, Mexico City, 2018.
26 S. Chiodo, N. Russo and E. Sicilia, Newly Developed Basis Sets for Density Functional Calculations, *J. Comput. Chem.*, 2005, **26**(2), 175–184.
27 Y.-F. Shen, C. Xu and L.-J. Cheng, Deciphering Chemical Bonding in $B_nH_n^{2-}$ (n = 2–17): Flexible Multicenter Bonding, *RSC Adv.*, 2017, **7**(58), 36755–36764.
28 I. Fernández, F. Cossío and M. A. Sierra, Dyotropic Reactions: Mechanisms and Synthetic Applications, *Chem. Rev.*, 2009, **109**, 6687–6711.